# Microscopic View of Charge Injection in an Organic Semiconductor

William R. Silveira and John A. Marohn

*Department of Chemistry and Chemical Biology, Cornell University, Ithaca, New York 14853-1301, USA*

(Received 18 May 2004; published 10 September 2004)

We have measured the chemical potential and capacitance in a disordered organic semiconductor by electric force microscopy, following the electric field and interfacial charge density microscopically as the semiconductor undergoes a transition from Ohmic to space-charge limited conduction. Electric field and charge density at the metal-organic interface are inferred from the chemical potential and current. The charge density at this interface increases with electric field much faster than is predicted by the standard diffusion-limited thermionic emission theories.

DOI: 10.1103/PhysRevLett.93.116104 PACS numbers: 68.37.–d, 73.30.+y, 73.61.Jc, 73.61.Ph

Organic electronic materials are particularly well suited for constructing high-efficiency solar cells and light emitting diodes [1], and cheap solution-processable thin-film transistors [2]. A fundamental understanding of how charge is injected from a metal to a $\pi$-conjugated organic system is essential to the design and operation of such organic electronic devices. Despite a growing body of phenomenological knowledge [3], a predictive microscopic theory of the charge injection process remains elusive [4].

Many theories have been proposed to describe charge injection into hopping transport materials. Early models were adapted from inorganic semiconductor injection theories such as Schottky injection and Fowler-Nordheim field emission. Recent theories have sought to describe the charge injection process as thermally assisted tunneling from the metal to localized states [5], tunneling into polaron levels in polymers [6], thermally-assisted injection into an energetically disordered dielectric [7], or as diffusion-limited thermionic emission [8,9]. Factors playing a role in metal-to-organic charge injection include the charge mobility in the organic layer [8–10], the dependence of the mobility on electric field [11] and on charge density [12,13], trapping of injected charges at the interface due to the image potential [14], interface dipoles arising from charge transfer [15] or interfacial chemistry [16], and disorder in these interface dipoles [17].

Testing microscopic theories of charge injection requires a separation of bulk and contact effects. One approach is to model the current-voltage behavior of devices of different length [18]. This is possible in systems in which the contact contributes significantly to the device resistance. In the case of a "good" contact, the device current is space charge limited and independent of the contact resistance. A more direct approach to disentangling bulk and contact effects has been to use conducting-probe potentiometry [19] and scanned probe potentiometry [20–22] to follow voltage drops in a working device. Studies of the temperature dependence of the poly(3-hexylthiophene)/metal contact resistance have recently led Bürgi *et al.* to call into question diffusion-limited thermionic emission theories [22].

In this Letter we use scanned probe potentiometry to investigate charge injection from a metal to a $\pi$-conjugated system through a *good* metal-organic contact, the behavior of which should provide a stringent test of thermionic emission theories of charge injection. We have studied the interface between gold and a triarylamine, N,N′-diphenyl-N-N′-bis(3-methylphenyl)-(1,1′-biphenyl)-4,4′-diamine (TPD), dispersed in polystyrene (PS). This system was chosen because bulk transport of holes in TPD-PS is well understood, is free of charge trapping effects [10,11,23], and has relatively well characterized interface energetics [16], and, most importantly, because this contact easily supports space-charge limited current (SCLC).

Samples were prepared in which a TPD-PS film conducts charge between two coplanar electrodes. Interdigitated gold electrodes were patterned on quartz by optical lithography. The source-drain gap was 5 $\mu$m, the length of each of the electrodes was 3 mm, and there were 67 electrodes in total. Electrodes were formed by evaporating a 50 Å adhesion layer of chromium followed by 500 Å of gold at a rate of 0.4 Å/s in high vacuum. The resulting metal films appeared polycrystalline by atomic force microscopy with a surface roughness of 0.65 nm. The quartz substrate was cleaned by sonication followed by UV/ozone treatment. Fifty weight percent TPD-PS was prepared by dissolving 15 mg of TPD (Xerox) and 15 mg of PS (MW $= 2.0 \times 10^6$, PD = 1.09; Aldrich) in 3 ml of dry tetrahydrofuran ($\leq 10$ ppm water) for 2.5 hours. The solution was spin cast in air onto the cleaned quartz substrates at 1900 rpm for 15 s, yielding amorphous films having a thickness of 100 nm and a surface roughness of 0.7 nm [Fig. 1(a)]. Samples were transferred into vacuum for characterization within an hour of preparation.

A measurement of current as a function of voltage appears to show a transition from Ohmic conduction at low voltages ($I_\Omega \propto V$) to SCLC at high voltages ($I_{\mathrm{SCL}} \propto V^2$), Fig. 1(b). At low voltages we expect a current density

  

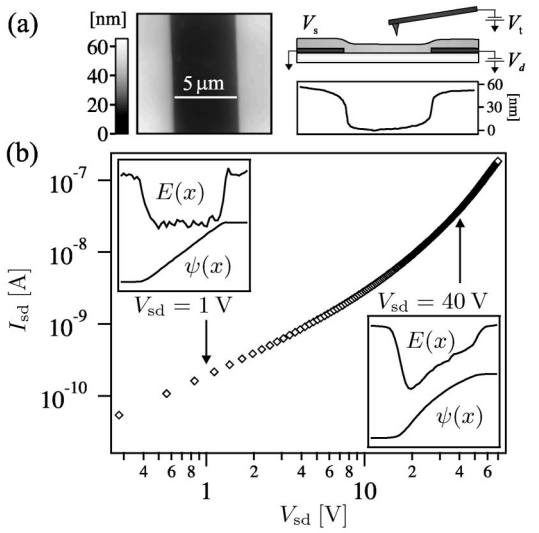


FIG. 1. TPD-PS sample topography and current-voltage curve. (a) Topographic image (left) and linescan (right), acquired by intermittent-contact atomic force microscopy. (b) Current $I$ versus applied source-drain voltage $V_{sd}$. The inset shows line scans of normalized chemical potential and electric field at low and high voltage.

$$J_\Omega = \mu_0 N_0 \frac{V}{L} e^{\beta\sqrt{V/L}}, \tag{1}$$

where $L$ is the channel length, $\mu_0$ is the zero-field mobility, $\beta$ accounts for the Poole-Frenkel-like field dependence of the mobility in TPD-PS [11,23], and $N_0$ is the density of free carriers. In the space-charge limit [24]

$$J_{SCL} = \frac{9}{8}\mu_0 \epsilon \frac{V^2}{L^3} e^{0.89\beta\sqrt{V/L}}, \tag{2}$$

where $\epsilon = 3\epsilon_0$ is the TPD-PS dielectric constant. We find that as $V \to 0$, $dI/dV$ is not zero, indicating an Ohmic current at low voltages. Above 2 V, both Eq. (1) and Eq. (2) fit the current equally well and we cannot distinguish Ohmic conduction from SCLC. The conduction mechanism(s) can, however, be unambiguously assigned using scanning potentiometry.

We imaged the chemical potential and tip-sample capacitance in TPD-PS/Au devices using a custom-built electric force microscope operating at room temperature in a vacuum of $10^{-6}$ mbar [25]. The microscope employs a Ti-Pt coated cantilever (model NSC21; MikroMasch) having a resonance frequency $f_0 = 28$ kHz, a spring constant $k = 1$ N/m, and a typical quality factor $Q = 2 \times 10^4$ in vacuum. Once the source-drain gap was located by intermittent-contact mode atomic force microscopy, the source was grounded and a voltage $V_{sd}$ was applied to the drain. The cantilever was scanned along a line 100 nm above the surface. At each position $x$ and $V_{sd}$ the cantilever resonance frequency $f$ was recorded while the cantilever tip voltage $V_t$ was varied. The cantilever was made the resonant element in a self-oscillating positive feedback loop [26]. The frequency of cantilever self oscillation was measured to a fractional accuracy of $\sim 10^{-7}$, for a drive amplitude of 20 nm and a gate time of 0.1 s.

The capacitive tip-sample force gradient leads to a resonance frequency of

$$f(V_t, x) = f_0 - \frac{f_0}{4k}\frac{\partial^2 C}{\partial z^2}(x)[V_t - \psi(x)]^2, \tag{3}$$

where $C$ is the tip-sample capacitance, $z$ is the tip-sample separation, and $\psi$ is the tip-sample chemical potential difference. Varying $V_t$ within $\pm 2$ V of $\psi$, $f$ was quadratic in $V_t$ to within a percent. Fitting $f$ to Eq. (3) we obtain $\partial^2 C/\partial z^2$ and $\psi$ vs $x$ and $V_{sd}$.

The potentiometry clearly illustrates the difference between the two conduction mechanisms. As seen in the left inset of Fig. 1, the chemical potential drops linearly from the injecting to extracting electrode. The electric field is uniform inside the device at low voltage, as expected for Ohmic conduction. At high voltages (right inset of Fig. 1), the potential reveals a nonuniform electric field, associated with a buildup of space charge. At all voltages there is no discernable voltage drop at the contacts. The potentiometry thus requires that Eq. (1) is the appropriate model at low voltages. We fit the current density from 0–2 V to $J_\Omega$ to determine the density of free charge carriers $N_0$, ignoring the electric field dependence of the mobility by setting $\beta = 0$. We then take $\mu_0 = 2 \times 10^{-9}$ m$^2$/Vs from Ref [23] and compute the current density as $J = I/A$ where $A = 1.1 \times 10^{-8}$ m$^2$ is the cross sectional area of the device assuming a sheet charge of height 55 nm (the contact height). We find $N_0 = 2.8 \times 10^{14}$ cm$^{-3}$; this value is independent of channel length (data not shown). The potentiometry also justifies fitting the data from 50–70 V to $J_{SCL}$; here we find $\mu_0 = 2.0 \times 10^{-9}$ m$^2$/Vs and $\beta = 0.60 \times 10^{-3}$(m/V)$^{1/2}$.

Although the chemical identity, concentration, and energy levels of the acceptor states giving rise to the bulk free carriers are not known, we can use Fermi-

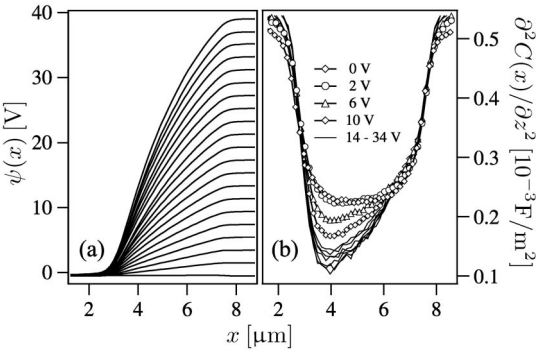


FIG. 2. (a) Chemical potential $\psi(x)$ versus distance $x$ across the source-drain gap. The source-drain bias $V_{sd}$ was varied from 0 to to 40 V. (b) Capacitance derivative for various $V_{sd}$.

Dirac statistics to determine the chemical potential of holes in the bulk TPD-PS from the measured density $N_0$ of bulk free carriers. Assuming a Gaussian density of highest occupied molecular orbitals (HOMO) of width $\sigma = 100$ mV,

$$N_0 = \frac{\rho}{\sqrt{2\pi\sigma^2}} \int_{-\infty}^{+\infty} \frac{\exp(-\varepsilon^2/2\sigma^2)}{1 + \exp[(\mu - \varepsilon_{\mathrm{HOMO}})/(k_B T)]} d\varepsilon \tag{4}$$

where $\rho = 2.66 \times 10^{20}$ /cm$^3$ is the concentration of TPD molecules. Numerically, we find $\mu - \varepsilon_{\mathrm{HOMO}} = 540$ mV.

Figure 2(a) shows the chemical potential $\psi(x)$ for $V_{\mathrm{sd}}$ varying from 2 to 40 V. The electric field, Figure 3(a), is obtained from the chemical potential: $E(x) = -d\psi/dx$. The constant slope of $E$ in the bulk implies a uniform charge density; we attribute this discrepancy with the standard Mott-Gurney prediction to deviations from the idealized one-dimensional conduction. The behavior of the electric field at the interface can be used to quantify the extent to which the current is space charge limited. If the injecting contact is supplying the material's space-charge limited current, then we expect the steady-state planar charge density in the material $\sigma_\epsilon$ to become comparable to that at the extracting electrode, $\sigma_L$, and much larger than that at the injecting electrode $\sigma_0$. By Gauss' law, $\sigma_L = \epsilon E_L$ and $\sigma_0 = -\epsilon E_0$, and by charge conservation, $\sigma_\epsilon = \epsilon(E_0 - E_L)$. A quantitative measure of the degree to which SCLC dominates transport is therefore $\eta \equiv -\sigma_\epsilon/\sigma_L = (E_L - E_0)/E_L$. As defined, $\eta = 0$ for purely Ohmic currents and $\eta = 1$ when the current is due purely to space charge. Figure 3(b) shows $\eta$ as a function of $V_{\mathrm{sd}}$. The data fits well to $\eta = \eta_\infty[1 - \exp(-V/V_0)]$ with $\eta_\infty = 0.667 \pm 0.007$; $V_0 = 10.0 \pm 0.4$ V, which agrees with a calculated crossover from $J_\Omega$ to $J_{\mathrm{SCL}}$ of 12 V.

The capacitance derivative, $\partial^2 C/\partial z^2$ [Eq. (3)], shown in Fig. 2(b), also evolves dramatically as the system undergoes the transition from Ohmic conduction to SCLC. The capacitance is large over the gold electrodes, and the general shape of the line scan reflects sample topography. However, the behavior of the capacitance between the source and drain suggests, rather surprisingly, that the bulk becomes depleted of free carriers near the extracting electrode as the space-charge limit is approached, leaving behind immobile charged acceptors, qualitatively shown in the inset of Fig. 3(b). A more detailed understanding of probe-sample capacitance is necessary in order to determine the free charge density.

By combining the current density with the local electric field, we can infer $\mu\rho = J/E$ at both injecting and extracting electrodes [Fig. 4(a)], where $\rho$ is the charge density. The observed exponential increase of $\mu\rho$ with $E$ cannot be explained by considering only the field dependence of the mobility. Including the Schottky-effect lowering of the injection barrier by the field gives a satisfactory description [Fig. 4(a), Fit 1]. The resulting injection barrier, $\phi_B = 360$ mV, is reasonable [Table I(A)]. The Schottky analysis is valid only at high fields, however, and assumes that equilibrium is reached via electron transfer from the metal to the empty HOMO states of the organic. This assumption does not hold for our sample.

From $\mu - \varepsilon_{\mathrm{HOMO}} = 540$ mV, calculated above, we have constructed the energy level diagram of Fig. 4(b). Equilibrium is reached between TPD and Au by transfer of electrons in the opposite direction, resulting in accumulation, not depletion, of holes near the interface. In this situation, the diffusion-limited thermionic emission theory of Emtage and O'Dwyer [8] is the most appropriate description of charge injection. We have revisited their model and derived an exact analytical equation for $\rho(E)$ at the injecting electrode valid at all fields [Table I(B)]. The fit to this theory [Fig. 4(a), Fit 2], with the injection barrier as the only free parameter, is poor. If we introduce, *ad hoc*, the measured density $N_0$ of bulk free carriers into the theory, the fit does not improve. Good agreement is achieved if we allow the Schottky exponent to vary [Table I(C)]; Fit 3 of Fig. 4(a) gives $\phi_B = 420$ mV

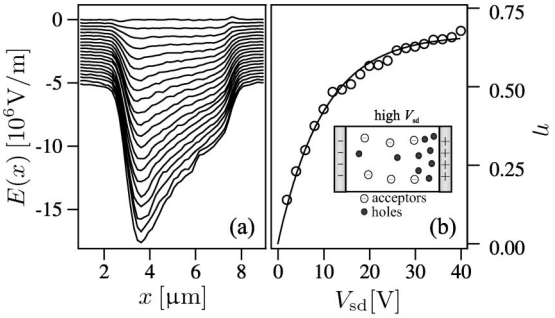


FIG. 3. (a) Electric field from source to drain. The source-drain bias $V_{\mathrm{sd}}$ is varied in 2 V steps from 0 to 40 V. For clarity, each curve has been offset vertically downward by $0.25 \times 10^6$ V/m from the $V_{\mathrm{sd}} = 0$ curve. (b) Degree to which SCLC dominates transport. (Inset) Free charge distribution.

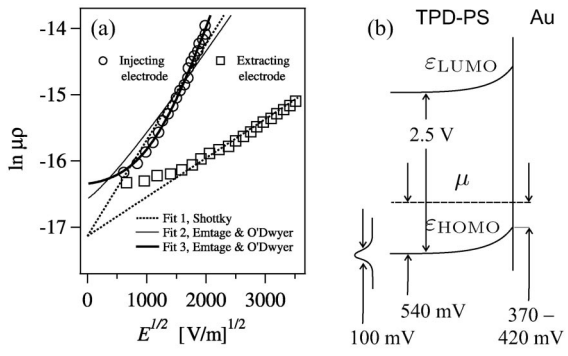


FIG. 4. (a) The charge density mobility product as a function of electric field for injecting and extracting electrodes. (b) Energy level diagram for the TPD-PS/Au interface.

TABLE I. Models used to describe $\mu\rho$. Both models account for the exponential field dependence of the mobility through the parameter $\beta_\mu = 0.60 \times 10^{-3}(\mathrm{m/V})^{1/2}$, inferred from $J_{\mathrm{SCL}}$. At the injecting electrode, the Schottky exponent was fixed at its theoretical value of $\beta_s = [q^3/4\pi\epsilon(kT)^2]^{1/2} = 0.85 \times 10^{-3}(\mathrm{m/V})^{1/2}$, while at the extracting electrode in A, $\beta_s$ was allowed to vary. The zero-field charge density $\rho_0 = \rho \exp[-\phi_B/(k_B T)]$ depends on the TPD density $\rho$ and on the injection barrier $\phi_B$; it was restricted to be the same at both electrodes in A. Here, $K_1$ is a modified Bessel function of the second kind.

| model | equation | parameter | injecting | extracting | units |
|---|---|---|---|---|---|
| A. Schottky (approximate) | $\mu_0\rho_0 \exp(\beta\sqrt{E})$ | $\beta = \beta_\mu + \beta_s$ | 1.45 | $0.590 \pm 0.012$ | $10^{-3}(\mathrm{m/V})^{1/2}$ |
| | | $\mu_0\rho_0$ | $36.2 \pm 1.2$ | | $10^{-9}$ A/Vm |
| B. Emtage & O'Dwyer | $\mu_0\rho_0 \exp(\beta_\mu\sqrt{E})/\beta_s\sqrt{E}K_1(\beta_s\sqrt{E})$ | $\mu_0\rho_0$ | $63.4 \pm 3.0$ | ⋯ | $10^{-9}$ A/Vm |
| C. Emtage & O'Dwyer | $\mu_0[\rho_0 \exp(\beta_\mu\sqrt{E})/\beta_s\sqrt{E}K_1(\beta_s\sqrt{E}) + N_0]$ | $\mu_0\rho_0$ | $8.1 \pm 0.6$ | ⋯ | $10^{-9}$ A/Vm |
| | | $\beta_s$ | $2.2 \pm 0.1$ | ⋯ | $10^{-3}(\mathrm{m/V})^{1/2}$ |

and $\beta_s = 2.2 \times 10^{-3}(\mathrm{m/V})^{1/2}$, approximately 2.6× larger than expected. While spatial averaging associated with a finite tip would lead to underestimating $E$ (and thereby overestimating $\beta_s$), this is unlikely considering that $E$ varies on a length scale much larger than our imaging resolution. Large $\beta_s$ has been observed in Monte Carlo simulations of charge injection incorporating energetic disorder [14].

In conclusion, we have examined charge injection and space charge in a disordered organic semiconductor by combining scanned probe microscopy and charge transport measurements. We have directly observed the transition from Ohmic to space-charge limited conduction, microscopically. Interfacial charge density was obtained from the measured current and inferred electric field. The charge density at this interface increases with electric field much faster than expected. We find that diffusion-limited thermionic emission theories, when strictly applied, do not completely describe the electric field dependence of the charge density at this well-studied metal-organic interface.

This work was supported by Cornell University, the National Science Foundation (via CAREER grant no. DMR-0134956, the Cornell Nanoscale Science and Technology Facility, and the Cornell Center for Nanoscale Systems), and the Eastman Chemical Company. TPD was kindly provided by the Xerox Corporation. The authors acknowledge Andronique Ioannidis, George Malliaras, and especially David Dunlap for many useful discussions.

[1] P. Peumans, A. Yakimov, and S. R. Forrest, J. Appl. Phys. **93**, 3693 (2003).
[2] H. E. Katz and Z. Bao, J. Phys. Chem. B **104**, 671 (2000).
[3] Y. L. Shen, A. R. Hosseini, M. H. Wong, and G. G. Malliaras, Chem. Phys. Chem. **5**, 16 (2004).
[4] J. C. Scott, J. Vac. Sci. Technol. A **21**, 521 (2003).
[5] M. A. Abkowitz and H. A. Mizes, Appl. Phys. Lett. **66**, 1288 (1995).
[6] E. M. Conwell and M. W. Wu, Appl. Phys. Lett. **70**, 1867 (1997).
[7] V. I. Arkhipov, E. V. Emelianova, Y. H. Tak, and H. Bässler, J. Appl. Phys. **84**, 848 (1998).
[8] P. R. Emtage and J. J. O'Dwyer, Phys. Rev. Lett. **16**, 356 (1966).
[9] J. C. Scott and G. G. Malliaras, Chem. Phys. Lett. **299**, 115 (1999).
[10] Y. Shen, M. W. Klein, D. B. Jacobs, J. Campbell Scott, and G. G. Malliaras, Phys. Rev. Lett. **86**, 3867 (2001).
[11] P. M. Borsenberger and D. S. Weiss, *Organic Photoreceptors for Xerography*, Optical Engineering (Marcel Dekker, Inc., New York, 1998).
[12] Y. Roichman and N. Tessler, Appl. Phys. Lett. **80**, 1948 (2002).
[13] C. Tanase, E. J. Meijer, P. W. M. Blom, and D. M. de Leeuw, Phys. Rev. Lett. **91**, 216601 (2003).
[14] Y. N. Gartstein and E. M. Conwell, Chem. Phys. Lett. **255**, 93 (1996).
[15] X. Crispin, V. Geskin, A. Crispin, J. Cornil, R. Lazzaroni, W. R. Salaneck, and J. L. Bredas, J. Am. Chem. Soc. **124**, 8131 (2002).
[16] M. Abkowitz, J. S. Facci, and J. Rehm, J. Appl. Phys. **83**, 2670 (1998).
[17] M. A. Baldo and S. R. Forrest, Phys. Rev. B **64**, 085201 (2001).
[18] B. H. Hamadani and D. Natelson, Appl. Phys. Lett. **84**, 443 (2004).
[19] K. Seshadri and C. D. Frisbie, Appl. Phys. Lett. **78**, 993 (2001).
[20] T. Hassenkam, D. R. Greve, and T. Bjørnholm, Adv. Mater. **13**, 631 (2001).
[21] L. Bürgi, H. Sirringhaus, and R. H. Friend, Appl. Phys. Lett. **80**, 2913 (2002).
[22] L. Bürgi, T. J. Richards, R. H. Friend, and H. Sirringhaus, J. Appl. Phys. **94**, 6129 (2003).
[23] H. J. Yuh and D. M. Pai, Mol. Cryst. Liq. Cryst. **183**, 217 (1990).
[24] P. N. Murgatroyd, J. Phys. D **3**, 151 (1970).
[25] W. R. Silveira and J. A. Marohn, Rev. Sci. Instrum. **74**, 267 (2003).
[26] T. R. Albrecht, P. Grütter, D. Horne, and D. Rugar, J. Appl. Phys. **69**, 668 (1991).